https://doi.org/10.5194/egusphere-2025-4275
Preprint. Discussion started: 17 October 2025

Characterizing runoff response to rainfall in permafrost catchments and its implications for hydrological and biogeochemical fluxes in a warming climate

Cansu Culha[1], Sarah Godsey[2], Shawn Chartrand[3], Melissa Lafrenière[4], James McNamara[5], James Kirchner[6],[7]

[1] Department of Earth, Ocean and Atmospheric Sciences, University of British Columbia, Vancouver, BC V6T 1Z4, Canada
[2] Department of Geosciences, Idaho State University, Pocatello, ID 83209, USA
[3] Department of Geography, Simon Fraser University, Burnaby, BC V5A 1S6, Canada
[4] Department of Geography and Planning, Queen's University, Kingston, ON K7L 3N6, Canada
[5] Department of Geosciences, Boise State University, Boise, ID 83725, USA
[6] Department of Environmental Systems Science, ETH Zürich, Zürich, 8092, Switzerland
[7] Swiss Federal Research Institute WSL, Birmensdorf, 8903, Switzerland

Correspondence to: Cansu Culha (cansu.culha@gmail.com) & James Kirchner (kirchner@env.ethz.ch)

Key Points (will be deleted; for personal reference):

1. Peak runoff response to rainfall is more than 5× stronger under wetter antecedent conditions in an Arctic permafrost catchment

2. Active layer detachments amplify rainfall-driven runoff and material fluxes at an Arctic permafrost catchment

3. Year-to-year variations in peak runoff response are associated with annual variations in average summer rainfall, antecedent winter and spring temperatures, and active layer detachment activity

---

Abstract
Understanding how Arctic catchments respond to rainfall is critical for anticipating hydrological and biogeochemical effects of a warming climate. We use ensemble rainfall-runoff analysis (ERRA) to identify how runoff response to rainfall varies with meteorological, subsurface, and geomorphic conditions across three permafrost catchments: Upper Kuparuk (Alaska) and the Goose and Ptarmigan catchments (Cape Bounty, Canadian High Arctic). ERRA enables us to quantify event-scale runoff responses to rainfall using high-resolution, multi-year hydrometeorological datasets, and test how variations in rainfall intensity, thaw depth, antecedent wetness, and active layer detachments (ALDs) affect runoff behavior. Our results show that peak runoff response increases by more than five-fold in response to increases in antecedent streamflow (a proxy for antecedent moisture), and is also higher in summers with higher

https://doi.org/10.5194/egusphere-2025-4275
Preprint. Discussion started: 17 October 2025

average precipitation. By contrast, warmer winters and springs, likely linked to deeper thaw and increased subsurface storage capacity, are associated with reduced runoff sensitivity to rainfall. Furthermore, a paired watershed comparison shows that streamflow and riverine fluxes of dissolved solids, suspended sediment, and particulate organic carbon are more readily mobilized by rainfall inputs when ALDs are present. Considered together, these findings highlight the difficulty in generalizing climate-driven runoff trends in permafrost regions subject to competing and interacting controls, such as precipitation intensity, storage capacity and permafrost stability. Our findings offer a more nuanced alternative to broad classifications of Arctic landscapes as “drying” or “wetting” under climate change.

Short Summary

We study how Arctic rivers respond to rainfall in a warming climate. We show that runoff response can increase more than 5x under wetter conditions, and Active Layer Detachments (ALDs) amplify water and material runoff response to rainfall. Increasing subsurface storage can reduce runoff sensitivity to rainfall. Our results inform the flashiness of rainfall-runoff predictions based on expected weather and erosion conditions.

1 Introduction

Catchments that are underlain by seemingly impermeable permafrost (land frozen for at least two consecutive years; Everdingen, 1998) can rapidly transport rain, snowmelt, melt waters from ground ice and glaciers to downstream waters (Levy et al., 2011; McNamara et al., 1999; Woo, 1982). With climate warming, the active layer that cyclically freezes and thaws above the permafrost is expected to become thicker (Wang et al., 2021; Levy et al., 2011; Wang et al., 2021; Jorgenson et al., 2010), altering subsurface flow patterns and increasing near-surface groundwater circulation and storage capacity (Walvoord & Kurylyk, 2012; Velicogna et al., 2012; St. Jacques & Sauchyn, 2009; Smith et al., 2007; Walvoord & Striegl, 2007; Frampton et al., 2015; McNamara et al., 1997). These changes are also expected to alter transport rates and timescales of both organic and inorganic terrestrial material (Beel et al., 2020; Beel et al., 2021; Toohey et al., 2016; Stieglitz et al., 2003; Coch et al., 2018; Spence & Woo, 2015; De Boer et al., 2016; Crowther et al., 2016). To better understand how climate change may affect solute and sediment transport in Arctic streams, we investigate how streamflow response to rainfall is shaped by precipitation intensity and ambient conditions. Climate change projections suggest that Arctic precipitation will increase in coming decades, with increasing prevalence of rainfall relative to snowfall (Bieniek et al., 2022; Bintanja et al., 2020; Bintanja & Andry, 2017). However, it is unclear whether these changes will lead to higher peak flows, and thus flashier flood responses, or whether these effects will be damped by deeper permafrost thaw and thus increases in subsurface storage capacity.

Understanding how climatic shifts may change the timing and magnitude of peak streamflow is challenging due to confounding effects of changing precipitation patterns, increasing storage, and accelerating landscape erosion. For example, it has been argued that deeper cycles of freezing and thawing in a warmer climate, and the resulting increase in active layer thickness, are likely to increase granular, pore-scale storage capacity and thus decrease runoff intensity (Stieglitz et al., 2003; Scherler et al., 2010; Stähli et al., 1999; Scherler et al., 2010).

Rainfall and snow/ice melt may also lead to greater saturation of pore-scale storage capacity, thus raising soil hydraulic conductivity, and making runoff more responsive to rainfall inputs (Stieglitz et al., 2003; Kurylyk et al., 2013). Some physical changes to the landscape, such as erosion of the active layer (Beel et al., 2020), may reduce subsurface storage capacity and thus accelerate and intensify runoff response.

https://doi.org/10.5194/egusphere-2025-4275
Preprint. Discussion started: 17 October 2025

Studying and quantifying each of these processes can be difficult because they can confound, amplify, or mask one another.

Ground-based observations, remote sensing data and modeling are commonly used to understand controls on streamflow dynamics. Each has its strengths and limitations. Ground-based observations show nuanced differences in runoff response between catchments and storms (e.g., McNamara et al., 1998; Kane et al., 2000; Stieglitz et al., 2003), but the extreme conditions in the Arctic make collecting long-term observational data difficult, with the result that few streams and rivers have been monitored continuously. For example, McNamara et al. (1998) investigated rainfall–runoff response over three years at four distinct catchment scales but faced challenges in identifying the causes of annual changes. Using remote sensing methods to resolve pore-scale subsurface characteristics in the Arctic remains challenging because the scales and extents of relevant processes are so dynamic (Walvoord & Kurylyk, 2016; National Research Council, 2014), despite recent advances (e.g., Michaelides et al., 2019; Pastick et al., 2013). Simulation models can explore how changing ambient conditions may alter multiple processes that shape runoff response in Arctic landscapes (Stieglitz et al., 2003; Evans et al., 2020). The mechanistic basis for such models remains incomplete, however, because we still do not adequately understand how permeability, hydraulic potentials, and subsurface storage capacity will change with rainfall intensity and contributions from snow/ice melt (e.g., Walvoord & Kurylyk, 2016; Kokkonen et al., 2004; Kurylyk et al., 2013; Chen et al., 2022).

Our study aims to characterize and quantify how summer runoff in landscapes underlain by permafrost is affected by precipitation intensity and antecedent wetness on timescales of hours to days, as well as precipitation and average temperatures during preceding seasons, the seasonal development of the active layer, and the erosion of the land surface. In this paper, "runoff" is understood to mean streamflow normalized by catchment area, potentially including both overland and subsurface flow. Our analysis makes use of multi-year time series data of runoff, precipitation, and temperature from the Upper Kuparuk River near Toolik Lake, Alaska, and the Goose and Ptarmigan catchments of Melville Island, Nunavut, Canada. We quantify the lagged response of runoff to rainfall, and examine how it varies with meteorological forcing and ambient catchment characteristics, yielding insight into the factors that amplify or dampen runoff response to precipitation.

Historically, runoff response to precipitation has often been characterized using unit hydrographs that capture the lagged response to precipitation events (Beven, 2012, page 456). However, unit hydrograph approaches are not well suited for quantifying the influence of factors such as rainfall intensity and antecedent wetness, because unit hydrographs typically assume runoff response is linear (i.e., proportional to precipitation) and stationary (i.e., independent of the ambient conditions when rain falls), whereas real-world runoff response is often nonlinear and nonstationary. Instead, we apply ensemble rainfall-runoff analysis (ERRA) (Kirchner, 2024), a data-driven, model-independent method for quantifying nonlinear and nonstationary rainfall-runoff relationships directly from time series data.

https://doi.org/10.5194/egusphere-2025-4275
Preprint. Discussion started: 17 October 2025

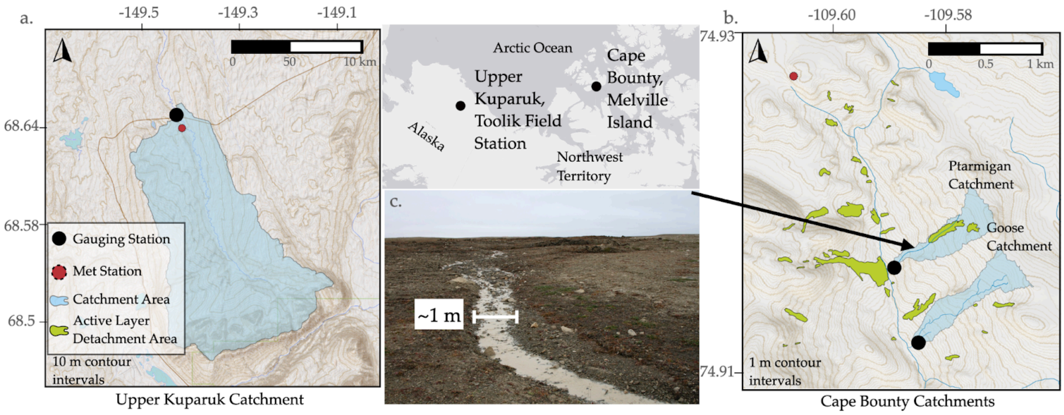

Figure 1. ***Maps of the permafrost catchments that inform this study.*** (a) Upper Kuparuk Catchment map near Toolik Field Station, northern Alaska; (b) Cape Bounty map with Ptarmigan and Goose catchments; (c) A photo of enhanced runoff from an active layer detachment (ALD) at Ptarmigan (stream is approximately 1m wide). Maps are generated using ArcticDEM data (Porter et al., 2018).

Using ERRA, we characterize the influence of processes modulating runoff response in permafrost landscapes on timescales of hours, months, and years. We conduct our analysis in the Upper Kuparuk (**Fig. 1a**) and Cape Bounty (Goose and Ptarmigan, **Fig. 1b**) catchments because they have multiple years of meteorologic, soil and streamflow data publicly available at 1-hour resolution. Furthermore, these catchments are relatively free of the confounding effects of glacial melt inputs (Kane et al., 2000). Additionally, the Ptarmigan catchment has two active layer detachments (ALDs; Lamoureux and Lafrenière, 2009), which are mass movements that initiate downslope sliding of the seasonally thawed active layer at the frozen-unfrozen interface, exposing the surface of the permafrost (the frost table) to the atmosphere (Paquette et al., 2020). Characterizing the role of ALDs in runoff response to rainfall provides a unique opportunity to understand how these thermoerosional features can impact runoff as permafrost destabilizes (**Fig. 1c**), which is critical because ALDs (Beel et al., 2021; Beel et al., 2020; Lafreniere et al., 2019; Beel et al., 2018) and other thermoerosional features are common (e.g., Gooseff et al., 2009; Yokeley et al., *in review)* and expanding (Balser et al., 2009; Biskaborn et al., 2019; Bowden et al., 2008; Krieger, 2012). Overall, the Upper Kuparuk, Goose and Ptarmigan catchments serve as natural laboratories for investigating the influence of meteorologic activity, active layer thaw depth and active layer detachment on permafrost runoff response.

---

2 Catchment descriptions and existing data

2.1 Upper Kuparuk

The Upper Kuparuk River (**Fig. 1a**) originates at 1,464 m a.s.l in the Brooks Range of northern Alaska and drains 142 km² at its outlet (68°38′24.5″ N and 149°24′23.4″ W, 778 m a.s.l.), where precipitation and streamflow have been recorded at hourly intervals since 2003 (Arp et al., 2017; Kane et al., 2021). Here we use data from 2005 and 2007–2017, since these years have a higher fraction of logged precipitation and streamflow data (see **Supp. Fig. 1a**). Hourly measurements are available for stream discharge (Onset Hobo U20 stage records, calibrated with biweekly discharge measurements using a Teledyne StreamPro Acoustic Doppler Current Profiler), precipitation (Texas Electronics TR-525M tipping bucket rain gauge),

https://doi.org/10.5194/egusphere-2025-4275
Preprint. Discussion started: 17 October 2025

air temperature (Vaisala HMP45C temperature sensor mounted at 1 m above ground), and soil temperature (Campbell Scientific CS615 and CS616 soil temperature probes). These high-frequency measurements are essential for our study, since the predominantly frozen subsurface conditions result in faster runoff response than is commonly observed in catchments that are dominated by deeper subsurface flow (McNamara et al., 1998; Newbury, 1974; Slaughter & Kane, 1983).

The Upper Kuparuk watershed is notable for its limited potential water sources, primarily precipitation and permafrost thaw. Unlike some other high-latitude basins, this catchment is not fed by large glaciers or aufeis, thereby limiting summer contributions largely to rainfall and permafrost thaw (McNamara et al., 1998). The catchment typically starts its flow season in May and discharges almost all of its snowmelt by June (Kane et al., 2000). Roughly two-thirds of summer precipitation leaves the catchment as streamflow (McNamara et al., 1998), implying that evapotranspiration is a relatively small component of the water balance. The relative simplicity of inputs and outputs allows for a focused analysis of the impacts of rainfall and thaw on permafrost hydrology.

During peak thaw in the Upper Kuparuk, continuous permafrost extends to 250–600 meters in thickness, with a roughly 50 cm active layer above it (Nelson et al., 1997; Arp et al., 2015; Kane et al., 2009; Kane et al., 1985), suggesting that there is no deep groundwater source feeding summer streamflow, which is instead derived from precipitation, melting permafrost and active layer ice, and flow through the active layer. This in turn implies that the characteristics of the permafrost and the active layer are critical for modulating streamflow.

2.2 Cape Bounty: Ptarmigan and Goose catchments

We also analyze two headwater catchments in the West River watershed of Cape Bounty Arctic Watershed Observatory (CBAWO), Melville Island in the Canadian High Arctic (74°54′ N, 109°35′ W; **Fig. 1b**). Similar to the Upper Kuparuk, the Cape Bounty catchments have multiple years of measurements taken daily or sub-daily between 2006 and 2018. However, data collection was not as consistent as at the Upper Kuparuk, limiting the types of analyses that are possible (**Supp. Fig. 1b–c**).

We focus on two adjacent headwater catchments at Cape Bounty: Goose (0.18 km^2) and Ptarmigan (0.21 km^2), both underlain by continuous permafrost without any glacial input. Unlike the Upper Kuparuk watershed, which is more vegetated, Cape Bounty has minimal vegetation and even lower amounts of precipitation: only roughly 160 mm of precipitation falls each year, mostly in the form of snow (Mekis & Hogg, 1999). The mean rainfall recorded at the Cape Bounty meteorological station between June and August for 2003–2023 was 45.4 ± 24.5 mm, with a minimum of 15.2 mm in 2014 and a maximum of 124.4 mm in 2019.

Although the neighboring Cape Bounty headwater catchments likely experience very similar meteorological and geologic controls, they do exhibit some important differences. Ptarmigan has two active layer detachments (ALDs), potentially because the average slope is slightly steeper: 3.9° at Ptarmigan versus 3.2° at Goose. The ALDs cover 10.8% of the surface area of Ptarmigan. The ALDs initiated in 2007 and the headwall retrogressively retreated over the next four years by a total of ~45±5 m, stabilizing at the end of the 2011 summer season (Beel et al., 2020). Although the retrogressive growth of these features may classify them as retrogressive thaw slumps in some literature, we follow the terminology used in previous Cape Bounty literature and refer to them as ALDs, distinguishing between periods of active growth (“active”) and quiescence (“stable”). We compare the runoff responses of the Ptarmigan and Goose catchments during periods when ALDs are active versus stable,

https://doi.org/10.5194/egusphere-2025-4275
Preprint. Discussion started: 17 October 2025

under the simplifying assumption that meteorological differences between the time periods exert a similar influence on both catchments.

At the Cape Bounty sites, the WestMet meteorological station provides hourly local temperature and rainfall data (Beel et al., 2018) at a hilltop north of the catchments (**Fig. 1b**). Discharge data was collected at gaging stations located at the outlet of the catchments, consisting of rectangular weirs (2006–2008) and 20 cm (8″) cutthroat flumes (2009–2017). They were equipped with Onset U20 (2006–2014) and vented Stevens SDX (2016–2017) pressure transducers to measure water level at 10-min intervals (Beel et al., 2020). Additionally, water samples were collected daily at each outlet, and analyzed for: (1) dissolved organic carbon (DOC) using a Shimadzu TOC-VPCH/TNM system (Fouché et al., 2017); (2) total dissolved solids (TDS), or major ion concentration, using ion chromatography, with individual cation and anion concentrations summed to derive TDS (Beel et al., 2020); (3) suspended sediment (SS), where samples were filtered through pre-weighed GF/F filters, which were then dried and reweighed to measure sediment mass per volume (Beel et al., 2020); and (4) particulate organic carbon (POC) by combusting the SS filters in a CHN elemental analyzer (Beel et al., 2020). We assess how material fluxes respond to precipitation in the two headwater catchments, with a focus on times when the ALDs are active.

---

3 Methods

We estimate how precipitation intensity and ambient conditions (including antecedent moisture, seasonal development of the active layer, and erosion of near-surface soils) affect streamflow response to precipitation using ensemble rainfall-runoff analysis (ERRA; Kirchner, 2024), a recently developed technique derived from general methods for estimating impulse responses in nonlinear, nonstationary, and heterogeneous systems (ERRA; Kirchner, 2022). ERRA uses multiple linear regression of precipitation and streamflow time series to estimate the ensemble-average response of streamflow to precipitation at the whole-catchment scale. For a given precipitation and streamflow time series, the simplest form of this linear regression is:

$$(1)\quad Q_i = \sum_{k=0}^{m} \beta_k P_{i-k} + c + \sigma_i,$$

where Q_i is streamflow, or runoff when normalized by catchment area, at the i-th time step, P_{i-k} is precipitation falling k time steps earlier, β_k is the impulse response function at lag k, c is the regression constant, and σ_i is the residual error associated with the runoff at hour i. Conventional linear regression analysis assumes that σ_i is white noise, but typical environmental time series are characterized by autocorrelated noise, so the approach outlined in Eq. (1) should not be applied directly in practice. Instead, as explained in Section 2 of Kirchner (2022), to account for the autocorrelation in σ_i, ERRA transforms Eq. (1) into:

$$(2)\quad Q_i = \sum_{l=1}^{h} \varphi_l Q_{i-l} + c + \xi_i \quad ,$$

(Equation 15 of Kirchner, 2022), where now β_k is the fitting coefficient, ϕ_l estimates the autocorrelation in the residuals σ_i from Eq. (1) for lags 1 to h ($h \leq m$), and ξ_i now represents uncorrelated white noise.

https://doi.org/10.5194/egusphere-2025-4275
Preprint. Discussion started: 17 October 2025

ERRA then uses both b_k and φ_l to estimate the original runoff response coefficients β_k using the recursion relationship (Equation 22 of Kirchner, 2022):

$$(3)\quad \beta_k = b_k + \sum_{l=1}^{min(k,h)} \beta_{k-l}\varphi_l$$

The coefficients β_k across a range of lags k comprise the Runoff Response Distribution (RRD), which estimates the ensemble average runoff response to a unit pulse of rainfall. The uncertainties in these coefficients will depend on the number of coefficients that need to be estimated from a given volume of data. To resolve the signal in the RRD while minimizing uncertainty, we aggregate the time steps, by averaging over different intervals to limit the number of coefficients that must be estimated.

To apply this approach at the Upper Kuparuk and Cape Bounty catchments, we assume that measured precipitation is rainfall if the temperature at the mean basin elevation is above 0°C. At the dry adiabatic lapse rate of 9.8°C per km, this corresponds to temperatures above 2°C at the Upper Kuparuk (where the weather station is located at the outlet, 200 m below the mean elevation), and above –0.5°C at Goose and Ptarmigan (where the weather station is located about 50 m above the mean basin elevation) (**Fig. 1**). We focus our analysis on summer rainfall events, rather than annual snowmelt or the occasional summer snowstorms.

The summertime hydrometeorological observations at Upper Kuparuk are mostly complete (data availability is >90% for any given year; **Supp. Fig. 1a**), facilitating analyses of how meteorological forcing and subsurface changes affect runoff. By contrast, data availability is ~50% for any given year at the Cape Bounty catchments (**Supp. Fig. 1b–c**), where we investigate how active layer detachments (ALDs) affect runoff response to rainfall.

At Upper Kuparuk, we test how the runoff response distribution changes with hourly rainfall intensity and antecedent streamflow (as a proxy for catchment-scale antecedent wetness), each year and each summer month (June, July, and August). We also test how the RRD varies with 12 candidate predictor variables: (1) total summer precipitation for the current and (2) previous summer; (3) total summer rainfall for the current summer; the (4) current and (5) previous summers' average rainfall intensities; (6) maximum snow depth and (7) total snowfall since the previous summer; (8) average temperatures during the preceding winter and spring; (9) average summer temperature; (10) cumulative degree days above C for the current summer, (11) maximum spring streamflow, and (12) the current summer's thaw rate. Because different fractions of data may be missing in individual years (**Supp. Fig. 1a**), we calculate total summer precipitation and rainfall as the average of the available data, multiplied by the combined duration of the three summer months. Winter and spring temperatures are calculated as averages from November 1 to May 31. The maximum pre-summer flood discharge is determined by identifying the highest runoff value in the daily time series from April 1 to May 31. The annual rate of subsurface thaw is calculated based on daily ground temperature data at 5 cm intervals down to 60 cm depth between 1994 and 2010. For each day, we set the thaw depth to be the deepest layer that is at or above 0°C. The snow depth and subsurface thaw rate data overlap with our precipitation and runoff records at Upper Kuparuk for only 5 years, precluding their use as long-term explanatory variables, but we use them as supplementary information to help interpret the results.

We evaluate each of the candidate predictors individually and the pairwise combinations of the 12 candidate predictors using two-variable multiple linear regressions. For each possible predictor pair, we

https://doi.org/10.5194/egusphere-2025-4275
Preprint. Discussion started: 17 October 2025

fit a linear model to the peak runoff response and calculate the resulting coefficient of determination (R^2). This allows us to assess how well these selected predictors jointly explain year-to-year peak runoff response.

To evaluate the individual contribution of each predictor to the peak runoff response to rainfall, we use added variable plots (Cook & Weisberg, 1982). These plots illustrate the partial relationship between each predictor and the response variable, after accounting for the influence of the other predictor in the model.

For all of these analyses at the Upper Kuparuk, we use runoff data obtained from Arp et al. (2017), precipitation data from Kane et al. (2021), snow depth data from Kane et al. (2021), and subsurface thaw data from Kane et al. (2021, updated), which we show over the period of record in **Supp. Fig. 2**.

One of the motivations behind exploring how changes in rainfall and thaw affect peak runoff is to better quantify and understand carbon and material mobilization. Since the ERRA approach can be applied to quantify the coupling between any interrelated time series, we can apply it to daily material fluxes at the Cape Bounty catchments. Instead of quantifying the overall annual increase in material concentrations in streams, as in Beel et al. (2020), the ERRA approach quantifies how much stream DOC, TDS, SS, and POC fluxes increase in response to rainfall, and how long these increases last. Given that the material flux data are only available for 92 individual days, we set the maximum response time to be 5 days (m = 5 days in **Eq. (1)**) to avoid overfitting.

---

4 Results and Discussion

We first analyze how runoff responds to short-term meteorological conditions, annual meteorological conditions, and increasing active layer thickness at Upper Kuparuk, given its longer and more complete record. We then investigate how ALDs affect rainfall-runoff behavior by comparing the Goose and Ptarmigan catchments when ALDs are active and stable. Finally, we quantify the material flux runoff response to rainfall at Goose and Ptarmigan.

4.1 Peak runoff response is sensitive to antecedent wetness

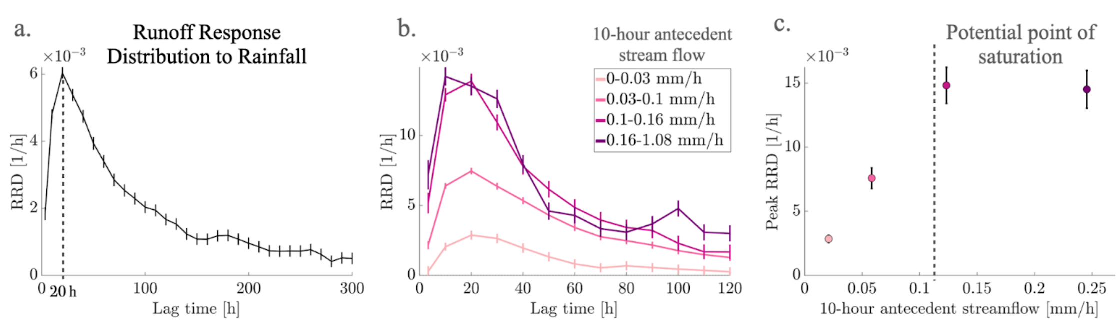

Figure 2. Runoff sensitivity to antecedent wetness at Upper Kuparuk. a. Average runoff response per unit rainfall at Upper Kuparuk (runoff response distribution using all available data, aggregated to 10-hour time steps); b. Runoff response distributions for different ranges of antecedent wetness, as proxied by 10-hour antecedent

https://doi.org/10.5194/egusphere-2025-4275
Preprint. Discussion started: 17 October 2025

streamflow; c. Peak height of runoff response distributions in (b), as a function of 10-hour antecedent streamflow. Peak runoff response increases approximately linearly with antecedent streamflow, up to an apparent saturation point indicated by the dashed line. Error bars indicate one standard error.

We initially examine runoff response to rainfall at Upper Kuparuk by considering the entire 14-year record of hourly data, aggregated into 10-hour time steps (**Fig. 2a**). The runoff response distribution (**Fig. 2a;** where the lag time is k and RRD is β in **Eq. (1)**) peaks approximately 20 hours after rain falls ($k = 2$ in **Eq. (1)**) and decays toward zero over the following 300 hours ($m = 30$ in **Eq. (1)**), with a runoff coefficient over this 300-hour period (the area under the RRD curve) of 57%. In other words, an equivalent of 57% of the rainfall is discharged over 300 hours. The peak of the runoff response distribution corresponds to 0.6% of the hourly rainfall rate (or an equivalent of 0.6% of the hourly rainfall discharges at the 20th hour), consistent with the duration of the runoff response.

To determine how antecedent wetness affects runoff response to precipitation, we compare runoff response distributions for different ranges of 10-hour lagged streamflow, as a proxy for antecedent catchment wetness (**Fig. 2b**). **Figure 2b** shows that higher levels of antecedent wetness yield a sharper and stronger peak runoff response, with these effects becoming asymptotic at relatively high antecedent wetness levels (**Fig. 2c**).

The five-fold increase in peak RRD with antecedent runoff is consistent with other permafrost catchments. For example, Dingman (1971) demonstrated that the intensity of runoff responses is correlated with antecedent discharge in 14 different storm events at the Glenn Creek watershed in the Tanana River Basin, Alaska. Antecedent runoff may serve as a proxy for antecedent wetness, as has been suggested in previous studies in temperate catchments (e.g., Massari et al., 2023; Knapp et al., 2024).

In **Fig. 2c**, the peak runoff response appears to plateau beyond a certain antecedent wetness threshold. We speculate that this behavior may reflect increasing subsurface saturation and routing of runoff as near-surface flow, consistent with observations at a smaller scale within the catchment (Rushlow and Godsey, 2017). One potential geomorphic expression of this process in permafrost landscapes is water tracks, narrow, linear features that concentrate surface or near-surface flow in permafrost landscapes (Del Vecchio and Evans, 2025; Evans et al., 2020). This saturation threshold may represent the point at which water tracks become hydrologically connected to stream channels, enabling efficient runoff without requiring full saturation of the entire landscape, consistent with modeling results within the basin (Stieglitz et al., 2003).

4.2 Peak runoff response increases linearly with precipitation intensity

https://doi.org/10.5194/egusphere-2025-4275
Preprint. Discussion started: 17 October 2025

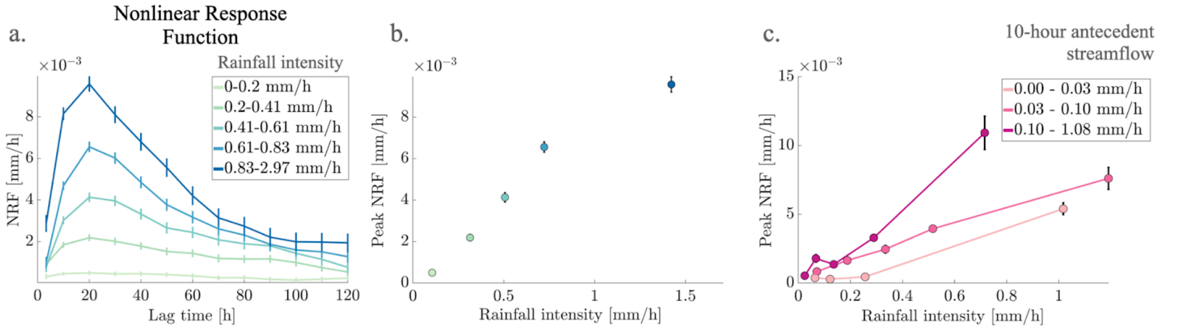

Figure 3. Runoff response at Upper Kuparuk increases linearly with rainfall intensity. a. Nonlinear response functions, depicting runoff response to precipitation falling within different ranges of precipitation intensity; b. Peak height of nonlinear response functions in (a) increases roughly linearly as a function of precipitation intensity; c. Peak height of nonlinear response functions for different ranges of antecedent wetness (indicated by the differently colored curves) and precipitation intensity. Higher antecedent wetness makes runoff more sensitive to precipitation intensity. All results obtained by aggregating hourly Upper Kuparuk time series to 10-hour intervals. Error bars indicate one standard error.

To assess how runoff response varies with rainfall intensity, we use the nonlinear response function (NRF; Kirchner, 2024), which equals the runoff response distribution for a given range of rainfall rates, multiplied by the time step and the rate of precipitation (**Fig. 3a**). The NRF measures the increase in streamflow resulting from one time step of precipitation at a given intensity. Whereas the RRD is a measure of runoff response per unit rainfall, the NRF is a measure of total runoff response per time interval of precipitation, and thus more clearly reveals how runoff response varies with precipitation intensity. As shown in **Fig. 3b**, higher rainfall intensities generate larger runoff responses as measured by the NRF. The peak height of the NRF increases approximately linearly with precipitation intensity.

Figure 3c shows how peak runoff response varies jointly as a function of precipitation intensity and antecedent wetness (indicated by the different curves, each corresponding to a different range of 10-hour antecedent streamflow). For each range of antecedent wetness (i.e., for each curve), peak runoff response is a weakly nonlinear function of rainfall rate. It is possible that runoff response becomes more strongly nonlinear at higher precipitation intensities than those shown here, but there are not enough of these events to robustly quantify the non-linearity at higher rainfall rates.

4.3 Stronger runoff response during wet summers, and following cold winters and springs

https://doi.org/10.5194/egusphere-2025-4275
Preprint. Discussion started: 17 October 2025

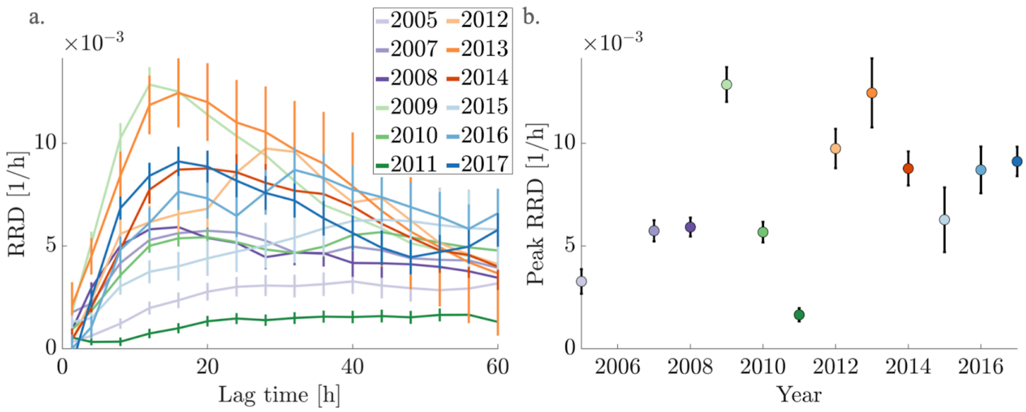

Figure 4. Year-to-year variability in runoff response distributions at Upper Kuparuk shows a sixfold range, with no clear temporal trend. a. Runoff response distributions for each year; b. Peak height of the distributions in (a) and their associated error bars plotted as a function of year. Each year is shown in a distinct color, used consistently throughout the manuscript. All results obtained by aggregating hourly Upper Kuparuk time series to 4-hour intervals. Error bars indicate one standard error.

Weather conditions vary from year to year at Upper Kuparuk, and their effects on runoff behavior can be illustrated by comparing runoff response distributions among individual years. The runoff response distributions for different years vary considerably, with some years exhibiting strong responses and others displaying weak responses (**Fig. 4**). For example, the peak runoff response distribution for 2009 corresponds to 1.3% of the hourly rainfall rate, whereas peak runoff responses in 2005 and 2011 correspond to less than 0.3% of the hourly rainfall rate (**Fig. 4**).

To evaluate the potential mechanisms behind this variability, we examine how year-to-year variations in runoff response reflect differences in both precipitation and temperature conditions, particularly those that influence subsurface storage capacity with the 12 potential explanatory variables outlined in the Methods section. The Methods section details how we measured each variable. In **Supp. Fig. 3,** we compare each explanatory variable individually with the peak runoff response to rainfall. Recall that because maximum snow depth and thaw rate data are only available for 5 rather than 12 full years, these two explanatory variables are only used to supplement our discussion.

Total current summer precipitation and rainfall (**Supp. Fig. 3a-b**) are first-order controls on peak runoff response to rainfall. Total summer precipitation includes all precipitation inputs, whereas rainfall refers specifically to those events that occur when air temperature exceeds 2°C.

The pair of predictor variables with the highest R^2 value in our multiple linear regression analyses is total summer precipitation and average temperatures during the preceding winter and spring. In **Fig. 5a**, we show the model fit for this best-performing pair. To facilitate interpretation and compare the relative influence of each variable, we standardized both predictors as z-scores and report the regression equation as:

$$(4)\quad z_{\beta} = (0.66 \pm 0.23)\, z_{P_s} - (0.46 \pm 0.23)\, z_{T_w} + c,$$

https://doi.org/10.5194/egusphere-2025-4275
Preprint. Discussion started: 17 October 2025

where z_β is the z-score–transformed peak runoff response to rainfall, z_{P_s} is the z-score–transformed total summer precipitation, z_{T_w} is the z-score–transformed average temperatures during the preceding winter and spring, and c is a baseline constant.

The added variable plots (**Fig. 5b-c)** show that the regression model performs fairly well (R^2= 0.58), and critically, it shows that both predictors are statistically significant: peak runoff response is influenced by both total summer precipitation (p=0.01) and average temperatures during the preceding winter and spring (p=0.03).

The correlation with summer precipitation is consistent with the patterns observed in **Figs. 2 and 3**, where peak runoff response shows a strong positive relationship with antecedent wetness and rainfall intensity. In addition to average summer precipitation, our analysis shows that average temperatures during the preceding winter and spring seasons are negatively correlated with runoff response (**Fig. 5**). These temperatures potentially reflect the extent and timing of subsurface thaw: warmer conditions during winter and spring may lead to earlier or deeper thawing, which would increase the capacity of the soil to absorb and store incoming water, leaving less water available for rapid runoff during summer rainfall events. In this way, average temperatures during the preceding winter and spring may serve as an indirect proxy for the thawed volume of the subsurface and the capacity of the catchment to buffer incoming precipitation.

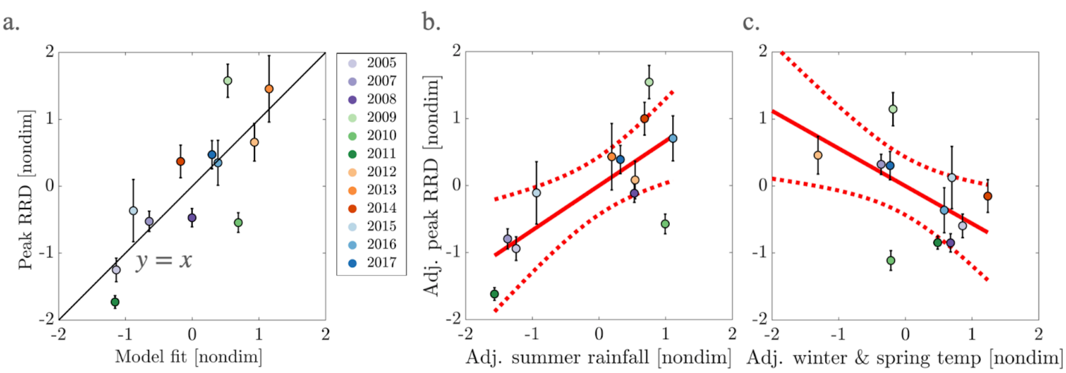

Figure 5. Factors influencing annual peak runoff response to rainfall at Upper Kuparuk. All variables shown as z-scores. a. Peak of the runoff response distribution for each summer, compared to fitted values of a linear model with total summer rainfall and average temperatures during the preceding winter and spring as explanatory variables. The diagonal line indicates a 1:1 relationship. b. Added variable plot (i.e., leverage plot) showing relationship between RRD peak height and total summer rainfall, corrected for linear effects of winter and spring temperatures. c. Added variable plot showing relationship between RRD peak height and winter and spring temperatures, corrected for linear effects of total summer rainfall. Error bars indicate one standard error.

4.4 Runoff is more sensitive to rainfall early than late in summer.

https://doi.org/10.5194/egusphere-2025-4275
Preprint. Discussion started: 17 October 2025

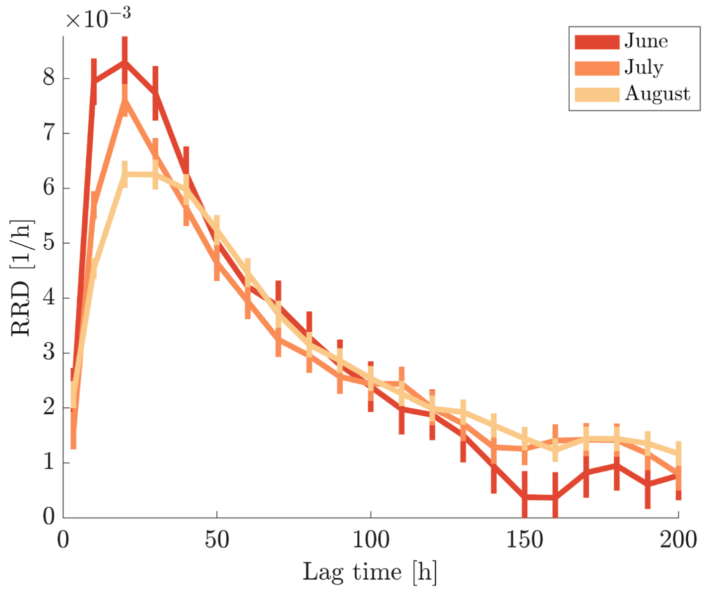

Figure 6. The Peak Runoff Response Distribution decreases by 25% between June and August at Upper Kuparuk. We show the runoff response distribution for June (red), July (orange) and August (yellow). All results obtained by aggregating hourly Upper Kuparuk time series to 10-hour intervals. Error bars indicate one standard error.

To further explore the role of thaw-related increases in subsurface storage capacity, we examine how runoff response changes over the course of the summer season. Specifically, we quantify the peak runoff response for each summer month to assess whether progressive thawing of the active layer influences runoff response.

Our analysis reveals a decline of approximately 25% in peak runoff response from June to August (**Fig. 6**). In **Supp. Fig. 4,** we show the monthly antecedent wetness response. Antecedent wetness can increase peak runoff response by a factor of three. Whereas the monthly decline in runoff response is modest compared to the variation driven by antecedent wetness, it provides insight into possible seasonal controls on runoff response.

To evaluate what drives this decline, we assess monthly changes in meteorological conditions in **Supp. Fig. 5**. Precipitation totals, air temperature, and rainfall intensity do not show consistent trends across the summer months, suggesting that changes in atmospheric forcing are unlikely to explain the decrease in peak runoff response. Similarly, seasonal variations in evaporation and transpiration do not align with the decline in runoff response: transpiration typically peaks in July and declines thereafter (Déry, et al., 2005), but the peak runoff response declines monotonically from June to August.

By contrast, active layer thaw depth increases substantially from June to August, expanding from approximately 20 cm to 50 cm on average at Upper Kuparuk Catchment (Shiklomanov, 2014). This increase in subsurface storage capacity potentially reduces the responsiveness of the catchment to rainfall by allowing more water to infiltrate and be stored rather than flow directly to the stream. As a

https://doi.org/10.5194/egusphere-2025-4275
Preprint. Discussion started: 17 October 2025

result, peak runoff response decreases. These findings support the hypothesis that seasonal expansion of subsurface storage capacity through thawing can decrease runoff response. This agrees with previous studies in the Upper Kuparuk where sequential storms through a summer had increasing old water contributions (McNamara et al., 1997), and lower runoff ratios (Q/P)(McNamara et al., 1998).

Although thawed-layer storage capacity over the summer months can influence runoff, its effect in the Upper Kuparuk appears secondary to other processes like antecedent wetness (**Fig. 2b-c**). In other catchments, thawed-layer storage capacity may play a more prominent role. Differences in soil texture and vegetation cover between catchments can cause hydraulic conductivity to vary by multiple orders of magnitude. On the timescale of peak runoff response in Upper Kuparuk (~24 hours), coarse, silty soils with permeabilities around 10^{-5} m/s can allow rainfall to infiltrate to depths on the order of tens of centimeters, comparable to the thickness of the active layer, enabling much of the precipitation to be stored in the subsurface. In contrast, clay-rich soils with permeabilities near 10^{-7} m/s may only permit infiltration of a few centimeters over the same period, quickly saturating the surface and generating more direct runoff.

This hypothetical example of two-order-of-magnitude difference in permeability, and the resulting disparity in infiltration depth, suggests that the importance of thawed-layer storage in regulating runoff will depend on topography, soil texture and hydraulic conductivity. Furthermore, where lateral conductivity exceeds vertical, water may drain efficiently downslope in some areas while pooling in others. These localized pools, due to the high heat capacity of water, can enhance thaw and generate spatial feedback in both storage capacity and runoff routing. In sum, the modest seasonal decline in peak runoff response (**Fig. 6**) likely reflects the combined effects of thaw depth, soil permeability, and anisotropic drainage, rather than the influence of thaw-layer storage alone.

4.5 Runoff response to rainfall increases when active layer detachments are active.

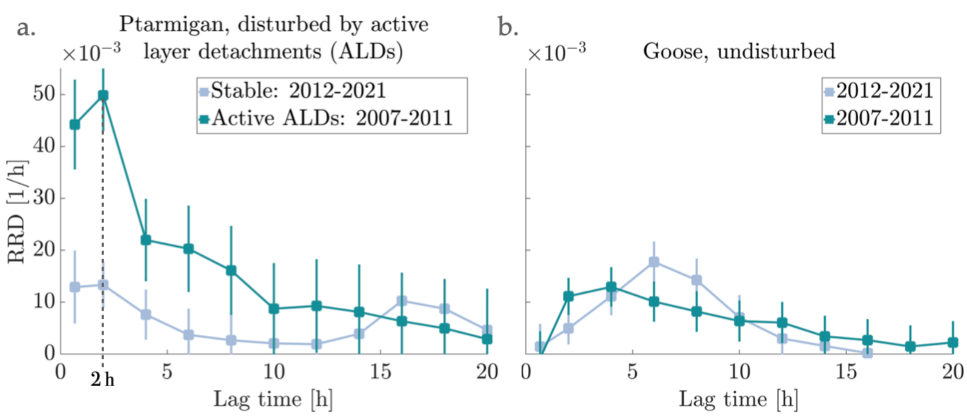

Figure 7. Runoff response distributions for Ptarmigan (a) and Goose (b). a. At Ptarmigan, active layer detachments disturbed ~10% of the catchment between 2007 and 2011. Runoff at Ptarmigan was more responsive to rainfall during this period (green) than during the following 10 years (2012-2021, blue). b. At the adjacent Goose catchment, where no active layer detachments were observed, runoff responses to rainfall were similar during

https://doi.org/10.5194/egusphere-2025-4275
Preprint. Discussion started: 17 October 2025

both periods. All results obtained by aggregating hourly Ptarmigan and Goose time series to 2-hour intervals. Error bars indicate one standard error.

To explore how erosion could alter the runoff response to rainfall in Arctic catchments, we analyze long-term data from the Cape Bounty region, which includes two neighboring catchments, Ptarmigan and Goose, of comparable size and climate. Two active layer detachments (ALDs) that initiated in 2007 disturbed roughly 10.8 % of the Ptarmigan catchment, stripping the upper unfrozen material along the main channel (**Fig. 1b**). The headwalls of the ALDs continued to erode through 2011, whereas the neighbouring Goose catchment remained geomorphically stable (Beel et al., 2021).

Figure 7 compares the runoff response to rainfall for both catchments, separating time periods with and without ALD activity. To isolate the effect of ALDs from meteorological variability, we compare runoff response at Ptarmigan before and after ALD activity, and contrast it with runoff response at Goose over the same time periods.

The results show that, on average, peak runoff response at Ptarmigan is four times higher during the five years with ALD activity (2007–2011) than during the 10-year post-ALD period (2012–2021). In contrast, the neighboring Goose catchment shows no significant difference in runoff response between the two time periods, suggesting that the changes in runoff response at Ptarmigan cannot be attributed to meteorological differences between the two periods. Moreover, the peak runoff response at Goose is about three times lower than at Ptarmigan during ALD-active years, reinforcing the inference that the changes at Ptarmigan are due to geomorphic disturbance rather than climate variability.

Although we lack pre-ALD data for Ptarmigan, the sharp decline in runoff response after stabilization suggests a strong effect of ALDs on runoff response. One plausible mechanism is that ALDs erode near-surface soil layers, exposing ice-rich permafrost (up to 80% ice by volume) with very low permeability (e.g., Paquette et al., 2020). This scar area may retain a shallower active layer for several years, reducing infiltration and enhancing surface runoff. Thus, although the ALDs area is only increasing by a few 10s of meters each active year, the large scar area can still have a significant impact on the runoff response.

After ALD stabilization, runoff response at Ptarmigan declines to roughly match the runoff response at Goose. We hypothesize that it is not the act of stabilization per se that reduces runoff, but rather the gradual thaw and drainage of the exposed ice-rich layer. As the active layer deepens and drains out pore water in the scar zone over time, increasing its capacity to store water. Further data on thaw depth within scar zones would help validate this hypothesis.

Alternatively, one could hypothesize that the causality runs in the opposite direction: that heightened runoff response triggers ALDs by lubricating subsurface layers, eroding scar-zone soils, or destabilizing headwalls. However, if this were the dominant mechanism, we would expect Goose to exhibit similarly elevated runoff response during 2007-2011. The lack of such elevated runoff response at Goose instead supports the hypothesis that ALD activity increased runoff response at Ptarmigan. The timing further supports this hypothesis. The years when ALDs were active, 2007–2011, also coincides with years when summer air temperatures were consistently above-average at Cape Bounty (Figure 1c in Beel et al., 2021). Warm conditions likely thawed an ice-rich layer, undermining slope stability and initiating the slides, which in turn amplified runoff by stripping away near-surface storage capacity. Thus, although high temperatures and elevated runoff could both potentially trigger ALD formation, the lack of elevated

https://doi.org/10.5194/egusphere-2025-4275
Preprint. Discussion started: 17 October 2025

runoff response at Goose supports the hypothesis that ALD formation and the associated loss of storage capacity drove the increase in runoff response at Ptarmigan during 2007-2011.

One important implication of the enhanced runoff response associated with ALDs is the potential to increase risks of flash floods and damage to critical infrastructure. Numerous ALDs and retrogressive thaw slumps have occurred along major transportation corridors in Canada, Alaska, and the Tibetan Plateau, resulting in significant damage and road closures (e.g., Ackerson et al., 2021; Van der Sluijs et al., 2018; Luo et al., 2021). Beyond the direct infrastructure damage that such thaw features cause, they can also generate long-lasting risks to infrastructure by intensifying the flashiness of rainfall-runoff events.

4.6 Catchments with ALD act as sources of biogeochemical and sediment export during rainfall

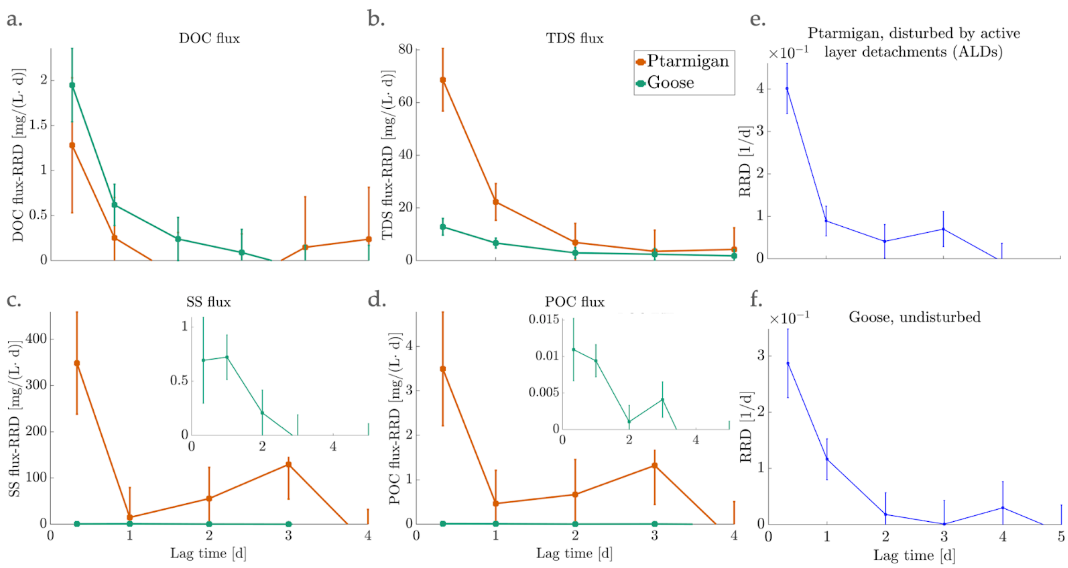

Figure 8. DOC, TDS, SSC, and POC runoff response distribution is comparable to water flux runoff response distribution to rainfall. Runoff response distributions quantifying how rainfall inputs increase runoff fluxes of dissolved organic carbon (DOC, panel a), total dissolved solids (TDS, panel b), suspended sediment (SS, panel c), and particulate organic carbon (POC) as inferred from suspended sediment concentrations (panel d). Subpanels in (c) and (d) zoom into the Goose SS flux-RRD and POC flux-RRD, respectively. Ptarmigan and Goose catchments are shown by orange and green lines, respectively. We compare these responses to water flux runoff response distribution to rainfall in panels e and f, which show similar temporal runoff response distributions. Error bars indicate one standard error.

Rainfall mobilizes solutes and sediments in addition to streamflow, and the relationships between rainfall inputs and the subsequent release of solutes and sediments may provide useful clues to catchment functioning. Frey et al. (2009), among others, have demonstrated dissolved organic carbon (DOC) levels tend to track the rise and fall of runoff from permafrost catchments. Koch et al. (2021), showed that DOC concentrations can remain elevated for multiple days following a rainfall event in two permafrost streams, leading to hysteresis in the concentration-discharge relationship. At Cape Bounty, Beel et al. (2018) observed increased suspended sediment (SS) transport in permafrost streams during storm events. Similarly, Lamoureux and Lafrenière (2014) reported that a single late-July storm contributed ~90% of the annual sediment load, highlighting the relative sensitivity of intact tundra to a single heavy rainfall event. Xiao et al. (2022) documented step-increases in both SS and total dissolved solids (TDS) in a permafrost headwater on the northeastern Tibetan Plateau during a storm that raised flows two orders of magnitude above baseflow values. Event-scale mixing analyses from the Upper Kuparuk River in Alaska likewise reveal pronounced solute enrichment during summer rainfall (McNamara et al., 1998). Collectively, these studies demonstrate that material fluxes respond to rainfall, and may persist longer than previously expected.

Alongside rainfall/runoff data, Cape Bounty has multiple years of DOC, TDS, SS and particulate organic carbon (POC) concentration data collected in streamflow at approximately daily intervals (Beel et al. 2020). These concentration measurements enable a detailed event-scale analysis of how material fluxes in streamflow respond to rainfall at Cape Bounty. Here, we define material fluxes as concentrations times streamflow normalized by catchment area. In **Supp. Fig. 6**, we show the time series of material fluxes alongside rainfall and runoff time series data. As shown in Beel et al. (2020), when the ALDs are active, DOC fluxes are elevated at Ptarmigan, but they subsequently decline as the ALDs stabilize, such that Goose becomes the larger DOC source when the ALDs are stable. TDS fluxes are persistently higher at Ptarmigan and rise further while the slides are active. SS and POC fluxes at Ptarmigan increase by an order of magnitude during ALD activity, whereas both fluxes remain minimal at Goose throughout the record. In **Supp. Fig. 7**, we show how material fluxes are correlated with precipitation and discharge. This figure shows that there is no clear correlation between material fluxes and precipitation. In contrast, discharge is positively correlated with material fluxes, particularly for TDS, SS, and POC at Ptarmigan; note that because discharge is part of the material flux calculation, positive correlations are expected (unless concentrations decrease more-than-proportionally with increasing discharge). TDS, SS, and POC fluxes increase more steeply as a function of discharge at Ptarmigan than at Goose; by contrast, DOC response to increasing discharge is broadly similar between the two catchments.

We use ERRA to quantify how material fluxes respond to rainfall on event time scales at Ptarmigan and Goose. In this analysis, we substitute runoff in **Eqs. (1)–(2)** with material fluxes (concentration multiplied by runoff), while retaining precipitation (P) as the driver. **Figure 8** illustrates how runoff fluxes of DOC, TDS, SS, and POC respond to rainfall at Ptarmigan and Goose. **Figure 8** shows that both catchments exhibit notable DOC and TDS flux runoff responses that peak within a day of rainfall and decline over the subsequent two days. In **Figs. 8e** and **f**, we show the daily water flux runoff response distribution to rainfall, which produces a similar rapid response that declines over the course of two days. This implies that rainfall mobilizes DOC and TDS flux at these catchments. Together with the previous findings of Beel et al. (2020), our results support the conclusion that rainfall mobilizes DOC and TDS. If rainfall intensity and frequency increase as projected under climate change (Bieniek et al., 2022; Bintanja, 2020), stream DOC and TDS concentrations may increase (and thus stream DOC and TDS fluxes may increase more than proportionally to increases in discharge).

Beel et al. (2020) compared annual fluxes at Ptarmigan and Goose and showed that the annual DOC flux is consistently higher at Goose, suggesting that ALDs do not dramatically alter DOC levels. The similarity between the DOC flux runoff response for Ptarmigan and Goose in **Fig. 8a** suggests that the event-scale response at the two catchments is similar, at least on average across the sampled events during 2007-2021. This suggests that, while Beel et al. (2020) report higher DOC fluxes at Goose as compared to

https://doi.org/10.5194/egusphere-2025-4275
Preprint. Discussion started: 17 October 2025

Ptarmigan, their event-scale responses are comparable, with differences in baseflow fluxes potentially making up the difference.

The annual major ion (TDS) flux increased after the 2007 ALDs at Ptarmigan and remained high during the following years, a pattern that is absent at Goose (Beel et al., 2020). **Figure 8b** also shows that the event-scale response of TDS runoff fluxes to rainfall is four times higher at Ptarmigan than at Goose, suggesting that the ALDs increased the TDS runoff response to rainfall.

Annual Ptarmigan SS and POC fluxes rose by 15–30 fold in the first season after ALDs initiated and remained an order of magnitude higher than background levels for the 5 years when ALDs were actively eroding, a pattern that is absent at Goose (Beel et al., 2020). Furthermore, catchments with ALDs at Cape Bounty have POC-dominated stream carbon fluxes for more than 5 years after the initial disturbance (Beel et al., 2021). **Figures 8c-d** show notable responses of SS and POC fluxes at Ptarmigan, but not at Goose. This indicates that rainfall more readily mobilizes SS and POC fluxes at Ptarmigan than at Goose, likely due to ALDs. These results suggest that ALDs may elevate TDS, SS, and POC fluxes and impose a legacy effect for multiple years after a disturbance.

Unfortunately, the sparsity of the available data precludes a clear assessment of differences in runoff response between the periods when the ALDs were active versus stable at Ptarmigan (e.g., similar to the runoff response in **Fig. 7**). Material flux runoff responses may have been higher in 2007-2012, when the ALDs were active, but more extensive data would be needed to confirm this. For example, it is possible that DOC flux increased in 2007, when ALDs initiated, given the high DOC concentrations typically found in permafrost landscapes. However, as the scar zone transitioned to a zone of mineral sorption (Littlefair et al., 2017), DOC flux runoff response may have dropped below the levels observed in **Fig. 8a**, to give an average DOC flux runoff response that is similar to Goose. Following this logic, we infer that the higher TDS, SS, and POC flux runoff response at Ptarmigan is either due to ALDs, when their flux runoff response was particularly high in 2007 or, more plausibly and consistent with annual data (Beel et al., 2018; 2020), remained elevated for several years following ALD initiation.

Our analysis extends understanding of the role of rainfall in mobilizing material transport by demonstrating ALDs in catchments like Ptarmigan may exert a sustained influence on rainfall-driven transport of major ions, suspended sediments, and particulate organic carbon, potentially even after landscape stabilization. Given projected increases in Arctic rainfall intensity and frequency, these prolonged effects could amplify the downstream impacts of ALD disturbances on aquatic systems.

5 Summary and implications for catchment behavior in a warming climate

https://doi.org/10.5194/egusphere-2025-4275
Preprint. Discussion started: 17 October 2025

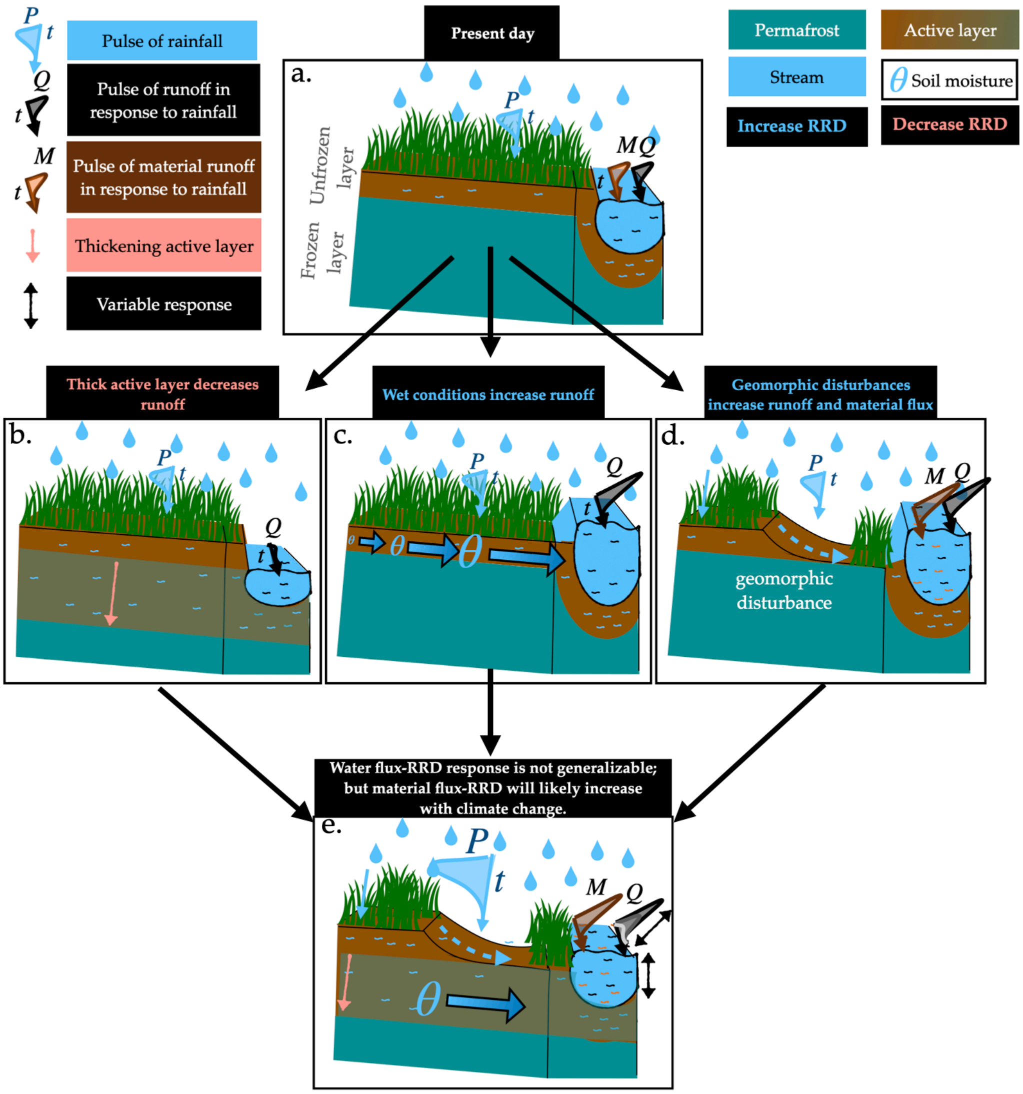

Figure 9. Conceptual model of processes influencing runoff response to rainfall in permafrost catchments. a. A conceptual model of the present day conditions at a landscape underlain by permafrost. The model shows a cross section of a catchment that has an active layer (brown) over permafrost (turquoise). Panel (a) shows the present day material and water flux runoff in response to a unit pulse of rainfall. As shown in the top left legend, arrows with a curve indicate the time (t) dependent component of rainfall (P) and runoff (Q, M). The blue curved arrow is to show a unit pulse of rainfall. The brown and black curved arrows are to show water (Q) and material (M) flux runoff response, respectively, to a unit pulse of rainfall. The magnitude of the curve indicates the intensity of rainfall or the intensity of runoff response. We summarize our results on how these runoff responses may vary in b-d. b. Thawing of the subsurface can increase storage capacity and thus decrease runoff sensitivity to rainfall. c. Whereas, rainfall increases soil moisture (θ) and thus makes runoff more responsive to rainfall. d. Erosion by active layer detachments (ALDs) can reduce subsurface storage capacity, making runoff more responsive to rainfall. ALDs may also act as sources of persistent biogeochemical and sediment export (**Fig. 8**). e. These competing and

https://doi.org/10.5194/egusphere-2025-4275
Preprint. Discussion started: 17 October 2025

interactive controls, considered alongside a future in which some regions will experience thicker active layers (pink arrow), increased rainfall (large curved blue arrow), and greater erosion, makes it difficult to generalize climate-driven water-flux runoff trends. We show this variability in runoff response to different controls with a double arrow line next to (1) the runoff response arrow and (2) the water levels. We also use different shades of gray about the runoff response arrow to illustrate the change in magnitude of the response. Regions that are prone to erosion by ALDs will see an increase in material-flux runoff with rainfall.

We summarize our results and their implications in a conceptual model in **Fig. 9**. Rainfall is represented by a curved blue arrow, resembling a time-series pulse. Both material (M; brown) and water (Q; black) fluxes respond to this pulse with increases illustrated by curved arrows, resembling the runoff response through time. Panels (b–d) illustrate how runoff of water (Q) and material (M) in response to rainfall (P) varies with active layer thickness (**Fig. 9b**), soil moisture conditions (**Fig. 9c**), and geomorphic disturbances (**Fig. 9d**).

The patterns captured in this model reflect the detailed results shown in earlier figures. **Figure 6** suggests that an increase in storage through the summer months decreases runoff response to rainfall over the course of the summer. Year-to-year variations in peak runoff response to rainfall are negatively correlated with average temperatures during the previous winter and spring (**Fig. 5**). These temperatures serve as a proxy for how rapidly the subsurface can thaw. The thickness of the thawed layer may increase the subsurface water storage potential and dampen peak runoff responses during the summer. In contrast, year-to-year variations in peak runoff response to rainfall are positively correlated with average summer precipitation (**Fig. 5).** Soil moisture can significantly influence runoff sensitivity to rainfall; as shown in **Fig. 2b-c**, different levels of antecedent catchment wetness (as reflected in different levels of antecedent streamflow) result in almost five-fold differences in peak runoff response to rainfall. We also use data from Cape Bounty to test how ALD activity affects runoff response to rainfall. **Figure 7** shows that during years when the ALD is actively eroding, runoff is more sensitive to rainfall. Finally, in **Fig. 8**, we show that DOC, TDS, SS, and POC fluxes respond to rainfall within a day; our results also reinforce earlier indications (Beel et al., 2020) that ALD activity may lead to long term biogeochemical and sediment export.

Projecting permafrost hydrology under climate change requires understanding how streamflow sensitivity to rainfall is shaped by precipitation patterns, temperature trends, and erosional processes. Arctic climate projections anticipate both increased precipitation and warmer temperatures (Tebaldi et al., 2006; Bintanja et al., 2020). In Alaska, precipitation is expected to increase by 14–25% between 2020 and 2049 (Bieniek, 2022; Bintanja et al., 2020), with most of the increase occurring as summer rainfall, given that snowfall is not projected to change significantly (Bintanja et al., 2017). Average winter temperatures are anticipated to rise by 3 °C over the next three decades (Bigalke et al., 2022). **Figure 5** suggests that it will be difficult to predict the net effect of these two trends, because they are comparably influential (e.g., z-scores of 0.66 vs. 0.46 in **Eq. (4)**), but have opposite effects on runoff sensitivity to rainfall. Interannual variability in runoff response is also significant (**Fig. 4**), underscoring the need for year-specific predictive modeling and cautioning against broad classifications of climate-driven drying or wetting trends (e.g., Qiu, 2012; Feng et al., 2021; Osuch, et al., 2022). We illustrate this variability in runoff response to climate change with a conceptual model (Fig. 9e). Rainfall is shown as a curved blue arrow resembling a time-series pulse, while the runoff response (Q) is depicted with arrows of varying magnitude. A double-headed arrow highlights the potential range of responses, emphasizing that future changes in rainfall sensitivity will depend on the interplay between increasing rainfall and warming temperatures.

https://doi.org/10.5194/egusphere-2025-4275
Preprint. Discussion started: 17 October 2025

In addition to rainfall and temperature increases, permafrost thaw will likely intensify erosional activity such as ALDs. Our results show that runoff response to rainfall can be amplified during years with active ALDs. By enhancing the flashiness of rainfall-runoff events, ALDs may increase the risk of flood-related damage to critical infrastructure in affected catchments.

Our results contribute to the ongoing discussion of how permafrost catchments are likely to respond to future climate changes. Beyond such generalized projections, however, our results can also inform year-by-year predictions based on expected weather conditions. For example, a wet summer following a cold winter is likely to yield strong runoff responses to rainfall. Similarly, a warm summer triggering ALDs may further amplify those responses. This framework provides tangible insights into which years may experience hydrologic wetting or drying, offering a more actionable alternative to broad climate impact assessments in permafrost landscapes.

Author contributions

CC and JWK contributed to conceptualization (formulation of research goals and aims) and methodology (development and design of methods, creation of models). CC carried out the formal analysis, investigation, writing – original draft preparation, and visualization. SG and ML were responsible for data curation. All authors contributed to writing – review and editing.

Acknowledgements

CC received funding from the National Science Foundation through the EAR Postdoctoral Fellowship Program.

Data availability. The datasets and scripts used in this study are publicly available at https://github.com/cculha4/Permafrost_ERRA_Toolik_Bounty. This repository includes all code required to reproduce manuscript results, processed data for the Upper Kuparuk, Goose, and Ptarmigan catchments, and the main figures.

Competing interests. The authors declare that they have no conflict of interest.

References

Ackerson, C. M., Ward, B., & Kennedy, K. (2021). Surficial geological mapping of the central Kluane ranges (parts of nts 115g/1, 2, 3, 7 and 115b/15, 16), Southwestern Yukon. *Yukon Exploration and Geology 202, KE MacFarlane (ed.)*, 157–176.

Arp, C., Kane, D., Stuefer, S., & Hinzman, L. (2017). *Hydrographic data, Upper Kuparuk River watershed, Alaska, 1993-2017.* Arctic Data Center. doi: 10.18739/ A29P2W61J

Arp, C., & Stuefer, S. (2022). *Climate data from the terrestrial environmental observation network (teon), arctic landscape conservation cooperative.* (Fairbanks, Alaska, variously paged. Retrieved on November 10, 2022)

Balser, A. W., Jones, J. B., & Gens, R. (2014). Timing of retrogressive thaw slump initiation in the Noatak Basin, northwest Alaska, USA. *Journal of Geophysical Research: Earth Surface*, *119*(5), 1106-1120.

Beel, C., Heslop, J., Orwin, J., Pope, M., Schevers, A., Hung, J., . . . Lamoureux, S. (2021). Emerging dominance of

https://doi.org/10.5194/egusphere-2025-4275
Preprint. Discussion started: 17 October 2025

summer rainfall driving high arctic terrestrial aquatic connectivity. *Nature Communications*, *12* (1), 1448.

Beel, C., Lamoureux, S., & Orwin, J. (2018). Fluvial response to a period of hydrometeorological change and landscape disturbance in the Canadian high arctic. *Geophysical Research Letters*, *45* (19), 10–446.

Beel, C., Lamoureux, S., Orwin, J., Pope, M., Lafrenière, M., & Scott, N. (2020). Differential impact of thermal and physical permafrost disturbances on high arctic dissolved and particulate fluvial fluxes. *Scientific Reports*, *10* (1), 11836.

Beven, K. J. (2012). *Rainfall-runoff modelling: the primer*. John Wiley & Sons.

Bieniek, P. A., Walsh, J. E., Fresco, N., Tauxe, C., & Redilla, K. (2022). Anticipated changes in Alaska extreme precipitation. *Journal of Applied Meteorology and Climatology, 61* (2), 97–108.

Bigalke, S., & Walsh, J. E. (2022). Future changes of snow in Alaska and the arctic under stabilized global warming scenarios. *Atmosphere*, *13* (4), 541.

Bintanja, R., & Andry, O. (2017). Towards a rain-dominated arctic. *Nature Climate Change*, *7* (4), 263–267.

Bintanja, R., van der Wiel, K., Van der Linden, E., Reusen, J., Bogerd, L., Krikken, F., & Selten, F. (2020). Strong future increases in arctic precipitation variability linked to poleward moisture transport. *Science advances*, *6* (7), eaax6869.

Biskaborn, B. K., Smith, S. L., Noetzli, J., Matthes, H., Vieira, G., Streletskiy, D. A., ... & Lantuit, H. (2019). Permafrost is warming at a global scale. *Nature communications*, *10*(1), 264.

Bowden, W. B., Gooseff, M. N., Balser, A., Green, A., Peterson, B. J., & Bradford, J. (2008). Sediment and nutrient delivery from thermokarst features in the foothills of the North Slope, Alaska: Potential impacts on headwater stream ecosystems. *Journal of Geophysical Research: Biogeosciences*, *113*(G2).

Chen, S., Fu, Y. H., Geng, X., Hao, Z., Tang, J., Zhang, X., . . . Hao, F. (2022). Influences of shifted vegetation phenology on runoff across a hydroclimatic gradient. *Frontiers in Plant Science*, *12,* 802664.

Coch, C., Lamoureux, S. F., Knoblauch, C., Eischeid, I., Fritz, M., Obu, J., & Lantuit, H. (2018). Summer rainfall dissolved organic carbon, solute, and sediment fluxes in a small arctic coastal catchment on Herschel island (Yukon Territory, Canada). *Arctic Science*, *4* (4), 750–780.

Cook, R. D., & Weisberg, S. (1982). *Residuals and influence in regression*. New York: Chapman and Hall.

Crowther, T. W., Todd-Brown, K. E., Rowe, C. W., Wieder, W. R., Carey, J. C., Machmuller, M. B., . . . others (2016). Quantifying global soil carbon losses in response to warming. *Nature*, *540* (7631), 104–108.

De Wit, H. A., Valinia, S., Weyhenmeyer, G. A., Futter, M. N., Kortelainen, P., Austnes, K., . . . Vuorenmaa, J. (2016). Current browning of surface waters will be further promoted by wetter climate. *Environmental Science & Technology Letters*, *3* (12), 430–435.

Dingman, S. L. (1971). Hydrology of the glenn creek watershed, tanana river basin, central Alaska.

https://doi.org/10.5194/egusphere-2025-4275
Preprint. Discussion started: 17 October 2025

Evans, S. G., Godsey, S. E., Rushlow, C. R., & Voss, C. (2020). Water tracks enhance water flow above permafrost in upland arctic Alaska hillslopes. *Journal of Geophysical Research: Earth Surface*, *125* (2), e2019JF005256.

Feng, D., Gleason, C. J., Lin, P., Yang, X., Pan, M., & Ishitsuka, Y. (2021). Recent changes to arctic river discharge. *Nature communications*, *12* (1), 6917.

Fouché, J., Lafrenière, M. J., Rutherford, K., & Lamoureux, S. (2017). Seasonal hydrology and permafrost disturbance impacts on dissolved organic matter composition in high arctic headwater catchments. *Arctic Science*, *3* (2), 378–405.

Frampton, A., & Destouni, G. (2015). Impact of degrading permafrost on subsurface solute transport pathways and travel times. *Water Resources Research*, *51* (9),7680–7701.

Frey, K. E., & McClelland, J. W. (2009). Impacts of permafrost degradation on arctic river biogeochemistry. *Hydrological Processes: An International Journal, 23* (1), 169–182.

Gooseff, M. N., Balser, A., Bowden, W. B., & Jones, J. B. (2009). Effects of hillslope thermokarst in northern Alaska. *Eos, Transactions American Geophysical Union*, *90*(4), 29-30.

Jorgenson, M. T., Romanovsky, V., Harden, J., Shur, Y., O'Donnell, J., Schuur, E. A., . . . Marchenko, S. (2010). Resilience and vulnerability of permafrost to climate change. *Canadian Journal of Forest Research*, *40* (7), 1219–1236.

Kane, D. (2022). *Climate data from the north slope hydrology research project.* http://www.uaf.edu/water/projects/NorthSlope/. (Fairbanks, Alaska, variously paged. Retrieved on November 10, 2022)

Kane, D., Hinzman, L., Gieck, R., Benson, C., Goering, D., McNamara, J., & Lilly, E. (2022). *Climate data from the north slope hydrology research project.* http://www.uaf.edu/water/projects/NorthSlope/. (Fairbanks, Alaska, variously paged. Retrieved on November 10, 2022)

Kane, D., Hinzman, L., McNamara, J., Zhang, Z., & Benson, C. (2000). An overview of a nested watershed study in arctic Alaska: Paper presented at the 12th northern res. basins/workshop (reykjavik, iceland–aug. 23rd-27th 1999). *Hydrology Research*, *31* (4-5), 245–266.

Kane, D., Hinzman, L., Stuefer, S., & Arp, C. (2021). *Updated meteorological, radiation, and soil temperature data, Kuparuk river and nearby watersheds: Upper Kuparuk (UK) station, 1994-2018.* Arctic Data Center. doi: 10.18739/A29P2W70H

Kirchner, J. W. (2022). Impulse response functions for nonlinear, nonstationary, and heterogeneous systems, estimated by deconvolution and demixing of noisy time series. *Sensors*, *22* (9), 3291.

Kirchner, J. W. (2024). Characterizing nonlinear, nonstationary, and heterogeneous hydrologic behavior using ensemble rainfall-runoff analysis (ERRA): proof of concept. *Hydrology and Earth System Sciences Discussions*, *2024,* 1–42.

Koch, J. C., Dornblaser, M. M., & Striegl, R. G. (2021). Storm-scale and seasonal dynamics of carbon export from a nested subarctic watershed underlain by permafrost. *Journal of Geophysical Research: Biogeosciences*, *126* (8), e2021JG006268.

Kokkonen, T., Koivusalo, H., Karvonen, T., Croke, B., & Jakeman, A. (2004). Exploring streamflow response to effective rainfall across event magnitude scale. *Hydrological Processes*, *18* (8),

https://doi.org/10.5194/egusphere-2025-4275
Preprint. Discussion started: 17 October 2025

1467–1486.

Kurylyk, B. L., & Watanabe, K. (2013). The mathematical representation of freezing and thawing processes in variably-saturated, non-deformable soils. *Advances in Water Resources*, *60*, 160–177.

Levy, J. S., Fountain, A. G., Goose, M. N., Welch, K. A., & Lyons, W. B. (2011). Water tracks and permafrost in taylor valley, antarctica: Extensive and shallow groundwater connectivity in a cold desert ecosystem. *Bulletin*, *123* (11-12), 2295–2311.

Lewis, T., Lafrenière, M. J., & Lamoureux, S. F. (2012). Hydrochemical and sedimentary responses of paired high arctic watersheds to unusual climate and permafrost disturbance, cape bounty, melville island, Canada. *Hydrological Processes*, *26* (13), 2003–2018.

Littlefair, C. A., Tank, S. E., & Kokelj, S. V. (2017). Retrogressive thaw slumps temper dissolved organic carbon delivery to streams of the Peel Plateau, nwt, Canada. *Biogeosciences*, *14* (23), 5487–5505.

Luo, J., Niu, F., Lin, Z., Liu, M., Yin, G., & Gao, Z. (2022). Inventory and frequency of retrogressive thaw slumps in the permafrost region of the Qinghai–Tibet Plateau. *Geophysical Research Letters*, *49* (23), e2022GL099829.

McNamara, J. P., Kane, D. L., & Hinzman, L. D. (1997). Hydrograph separations in an Arctic watershed using mixing model and graphical techniques. *Water Resources Research*, *33*(7), 1707-1719.

McNamara, J. P., Kane, D. L., & Hinzman, L. D. (1998). An analysis of streamflow hydrology in the Kuparuk River Basin, arctic Alaska: a nested watershed approach. *Journal of Hydrology, 206* (1), 39-57. Retrieved from https://www.sciencedirect.com/science/article/pii/S0022169498000833doi: https://doi.org/10.1016/S0022-1694(98)00083-3

McNamara, J. P., Kane, D. L., & Hinzman, L. D. (1999). An analysis of an arctic channel network using a digital elevation model. *Geomorphology, 29* (3-4), 339– 353.

Mekis, E., & Hogg, W. D. (1999). Rehabilitation and analysis of Canadian daily precipitation time series. *Atmosphere-ocean*, *37* (1), 53–85.

Michaelides, R. J., Schaefer, K., Zebker, H. A., Parsekian, A., Liu, L., Chen, J., . . . Schaefer, S. R. (2019). Inference of the impact of wildfire on permafrost and active layer thickness in a discontinuous permafrost region using the remotely sensed active layer thickness (ReSALT) algorithm. *Environmental Research Letters*, *14* (3), 035007.

National Research Council, Division on Earth, Polar Research Board, Committee on Opportunities to Use Remote Sensing in Understanding Permafrost, & A Workshop. (2014). *Opportunities to use remote sensing in understanding permafrost and related ecological characteristics: report of a workshop*. National Academies Press.

Nelson, F., Shiklomanov, N., Mueller, G., Hinkel, K., Walker, D., & Bockheim, J. (1997). Estimating active-layer thickness over a large region: Kuparuk river basin, Alaska, usa. *Arctic and Alpine Research*, *29* (4), 367–378.

Newbury, R. W. (1974). River hydrology in permafrost areas. In *Proc. workshop seminar on permafrost hydrology* (pp. 31–37). Ottawa, Ontario.

Osuch, M., Wawrzyniak, T., & Majerska, M. (2022). Changes in hydrological regime in high arctic non-glaciated catchment in 1979–2020 using a multimodel approach. *Advances in Climate Change*

https://doi.org/10.5194/egusphere-2025-4275
Preprint. Discussion started: 17 October 2025

Research, *13* (4), 517–530.

Pastick, N. J., Jorgenson, M. T., Wylie, B. K., Minsley, B. J., Ji, L., Walvoord, M. A., . . . Rose, J. R. (2013). Extending airborne electromagnetic surveys for regional active layer and permafrost mapping with remote sensing and ancillary data, Yukon Flats ecoregion, Central Alaska. *Permafrost and Periglacial Processes*, *24* (3), 184–199.

Porter, C., Morin, P., Howat, I., Noh, M.-J., Bates, B., Peterman, K., ... & Bojesen, M. (2018). *ArcticDEM* [Digital elevation model]. Harvard Dataverse. https://doi.org/10.7910/DVN/OHHUKH

Qiu, J. (2012). Thawing permafrost reduces river runoff. *Nature*, *6*.

Rovansek, R. J., Hinzman, L. D., & Kane, D. L. (1996). Hydrology of a tundra wetland complex on the Alaskan arctic coastal plain, usa. *Arctic and Alpine Research*, *28* (3), 311–317.

Rushlow, C. R., & Godsey, S. E. (2017). Rainfall–runoff responses on Arctic hillslopes underlain by continuous permafrost, North Slope, Alaska, USA. *Hydrological Processes*, *31*(23), 4092-4106.

Scherler, M., Hauck, C., Hoelzle, M., Stähli, M., & Völksch, I. (2010). Meltwater infiltration into the frozen active layer at an alpine permafrost site. *Permafrost and Periglacial Processes*, *21* (4), 325–334.

Shiklomanov, N. (2014). *Toolik mat: Active layer thickness grid measurements at Toolik, Alaska (site id: 229).*http://gtnpdatabase.org/activelayers/view/229.Retrieved from http://gtnpdatabase.org/activelayers/view/229 (Created: 2014-02-03; Last Updated: 2014-02-03. Data from the Circumpolar Active Layer Monitoring (CALM) program. Principal Investigator: Nikolay Shiklomanov, The George Washington University, Department of Geography.)

Slaughter, C. (1983). Summer streamflow and sediment yield from discontinuous permafrost headwaters catchments. In *Proc. 4th int. conf. permafrost, fairbanks, Alaska, 1983.*

Smith, L. C., Pavelsky, T. M., MacDonald, G. M., Shiklomanov, A. I., & Lammers, R. B. (2007). Rising minimum daily flows in northern eurasian rivers: A growing influence of groundwater in the high-latitude hydrologic cycle. *Journal of Geophysical Research: Biogeosciences*, *112* (G4).

Spence, C., Kokelj, S., Kokelj, S., McCluskie, M., & Hedstrom, N. (2015). Evidence of a change in water chemistry in Canada's subarctic associated with enhanced winter streamflow. *Journal of Geophysical Research: Biogeosciences*, *120* (1), 113–127.

Stähli, M., Jansson, P.-E., & Lundin, L.-C. (1999). Soil moisture redistribution and infiltration in frozen sandy soils. *Water Resources Research*, *35* (1), 95–103.

Stieglitz, M., Shaman, J., McNamara, J., Engel, V., Shanley, J., & Kling, G. W. (2003). An approach to understanding hydrologic connectivity on the hillslope and the implications for nutrient transport. *Global biogeochemical cycles*, *17* (4).

St. Jacques, J.-M., & Sauchyn, D. J. (2009). Increasing winter baseflow and mean annual streamflow from possible permafrost thawing in the northwest territories, Canada. *Geophysical Research Letters*, *36* (1).

Tank, S. E., McClelland, J. W., Spencer, R. G., Shiklomanov, A. I., Suslova, A., Moatar, F., . . . others (2023). Recent trends in the chemistry of major northern rivers signal widespread arctic change. *Nature Geoscience*, *16* (9), 789–796.

Tebaldi, C., Hayhoe, K., Arblaster, J. M., & Meehl, G. A. (2006). Going to the extremes: an intercomparison of model-simulated historical and future changes in extreme events. *Climatic change*, *79* (3-4), 185–211.

Toohey, R. C., Herman-Mercer, N. M., Schuster, P. F., Mutter, E. A., & Koch, J. C. (2016). Multidecadal increases in the Yukon river basin of chemical fluxes as indicators of changing flowpaths, groundwater, and permafrost. *Geophysical Research Letters*, *43* (23), 12–120.

Van der Sluijs, J., Kokelj, S. V., Fraser, R. H., Tunnicliffe, J., & Lacelle, D. (2018). Permafrost terrain dynamics and infrastructure impacts revealed by UAV photogrammetry and thermal imaging. *Remote Sensing, 10* (11), 1734.

Van Everdingen, R., Association, I. P., et al. (1998). *Multi-language glossary of permafrost and related ground-ice terms in chinese, english, french, german*. Arctic Institute of North America, University of Calgary.

Velicogna, I., Tong, J., Zhang, T., & Kimball, J. S. (2012). Increasing subsurface water storage in discontinuous permafrost areas of the lena river basin, eurasia, detected from grace. *Geophysical research letters*, *39* (9).

Voytek, E. B., Rushlow, C. R., Godsey, S. E., & Singha, K. (2016). Identifying hydrologic flowpaths on arctic hillslopes using electrical resistivity and self potential. *Geophysics*, *81*(1), WA225-WA232.

Walvoord, M. A., & Kurylyk, B. L. (2016). Hydrologic impacts of thawing permafrost—a review. *Vadose Zone Journal, 15* (6), vzj2016–01.

Walvoord, M. A., & Striegl, R. G. (2007). Increased groundwater to stream discharge from permafrost thawing in the Yukon River Basin: Potential impacts on lateral export of carbon and nitrogen. *Geophysical Research Letters*, *34* (12).

Walvoord, M. A., Voss, C. I., & Wellman, T. P. (2012). Influence of permafrost distribution on groundwater flow in the context of climate-driven permafrost thaw:

Example from Yukon Flat Basin, Alaska, United States. *Water Resources Research*, *48* (7).

Wang, K., Zhang, T., & Yang, D. (2021). Permafrost dynamics and their hydrologic impacts over the russian arctic drainage basin. *Advances in Climate Change Research*, *12* (4), 482–498.

Wang, P., Huang, Q., Pozdniakov, S. P., Liu, S., Ma, N., Wang, T., . . . others (2021). Potential role of permafrost thaw on increasing siberian river discharge. *Environmental Research Letters*, *16* (3), 034046.

Woo, M., & Steer, P. (1982). Occurrence of surface flow on arctic slopes, Southwestern Cornwallis Island. *Canadian Journal of Earth Sciences*, *19* (12), 2368–2377.